

---

# AN EVALUATION OF SELF-SUPERVISED PRE-TRAINING FOR SKIN-LESION ANALYSIS

---

A PREPRINT

**Levy Chaves<sup>1</sup> Alceu Bissoto<sup>1</sup> Eduardo Valle<sup>2</sup> Sandra Avila<sup>1</sup>**

<sup>1</sup>Institute of Computing (IC) <sup>2</sup>School of Electrical and Computing Engineering (FEEC)  
RECOD Lab., University of Campinas (UNICAMP), Brazil

November 13, 2021

## ABSTRACT

Self-supervised pre-training appears as an advantageous alternative to supervised pre-trained for transfer learning. By synthesizing annotations on pretext tasks, self-supervision allows to pre-train models on large amounts of pseudo-labels before fine-tuning them on the target task. In this work, we assess self-supervision for the diagnosis of skin lesions, comparing three self-supervised pipelines to a challenging supervised baseline, on five test datasets comprising in- and out-of-distribution samples. Our results show that self-supervision is competitive both in improving accuracies and in reducing the variability of outcomes. Self-supervision proves particularly useful for low training data scenarios ( $< 1500$  and  $< 150$  samples), where its ability to stabilize the outcomes is essential to provide sound results.

**Keywords** Self-supervision · Skin lesions · Melanoma · Classification · Dermoscopy · Small Datasets

## 1 Introduction

Self-supervised learning bridges the gap between supervised learning, which leads to the most accurate models but requires human-annotated samples, and unsupervised learning, which can exploit non-annotated samples but often leads to disappointing accuracies. By using synthesized annotations on so-called *pretext tasks*, self-supervision is able to *pre-train* models on abundant pseudo-labels before tuning them for the actual target task.

Applications for which annotated data is expensive or scarce — often the case for medical applications — especially benefit from self-supervision. Training state-of-the-art Deep Learning models require very large training datasets, which are seldom available for medical applications. We can mitigate the issue by applying transfer learning, i.e., pre-training the models (with classical supervised learning) on a large, unrelated dataset, and fine-tuning them on the target dataset, but there is a risk that the representations learned during pre-training will not fully adapt to the target task [23]. Self-supervised pre-training has proved, thus, advantageous for transfer learning in many tasks, such as object localization [17], speech representation [21], and medical image classification [36].

In this work, we assess self-supervision pre-training for the automated diagnosis of skin lesions, an application for which traditionally transfer learning from models supervised on ImageNet is employed to mitigate the scarcity of data [23, 32]. A couple of works [1, 33] have demonstrated the promise of self-supervision for skin-lesion analysis, but literature still lacks a systematic evaluation with our scope in terms of number of pipelines, datasets, and hyperparameters evaluated. In addition, ours is the first work to showcase the importance of self-supervised pre-training for very low training data scenarios (less than 150 samples in our most stringent test).

The main contributions of this work are:

- We assess five self-supervision learning schemes (BYOL [13], InfoMin [31], MoCo [14], SimCLR [8], and SwAV [6]) against a competitive supervised baseline;

- We perform a systematic assessment of four transfer learning pipelines (the supervised baseline and three self-supervised contenders) in five test datasets, comprising in-distribution and out-distribution scenarios;
- We assess the performance of our pipelines/datasets in a low-data training scenario (with as few as 148 samples).

We organized the remaining text as follows. We discuss the state-of-the-art on self-supervision in Section 2, comprising both general works and those dedicated to medical images, and to skin lesions in particular. We detail our goals, datasets, pipelines, protocols, experimental design, and implementation details in Section 3. Experimental results and analyses appear in Section 4. Finally, we discuss our main findings, along with future research directions in Section 5.

## 2 Related work

Self-supervised learning pre-trains models on auxiliary *pretext tasks* such as colorizing [35], predicting rotation angles [12], and in-painting [25], before fine-tuning them on the target task. This allows pre-learning representations on unlabeled data and then refining those representations on labeled data. In this section, we survey the most relevant techniques for this work, comprising the most important general-purpose techniques and those applied to medical images and skin-lesion images in particular. For a comprehensive survey on the field, we refer the reader to the work of Jing *et al.* [19].

### 2.1 Self-supervised learning techniques

A critical breakthrough on self-supervised learning was the adoption of contrastive losses [19, 30], which explicitly organized the feature space. Self-supervised contrastive learning brings together the representations for a positive pair of *views* from a single training sample, while pushing apart the representations for a negative pair of views from two different training samples. The scheme uses data augmentation to create the views, and requires no semantic annotation.

InstDis [34] was the seminal work on contrastive self-supervision. As explained above, InstDis reframed class-level classification as instance-level discrimination: each instance from the dataset becomes its own class, to be distinguished from all other instances. For instance-level discrimination, InstDis used a softmax classifier on  $\ell_2$ -standardized, 128-dimensional representation. It employed a memory bank (a mechanism used to store and sample feature pairs) to improve training stability and convergence.

SimCLR [8] improved InstDis by employing two multi-layer perceptrons to project the latent representations onto a 128-dimensional representation, and by applying heavy image augmentations, which it demonstrated to be crucial to learn good representations, easily transferable to other tasks. SimCLR required very large batch sizes of 4096 samples (*vs.* InstDis’ 256) obviating the storage of features in a memory bank.

MoCo [14] proposed a pretext task based on dynamic dictionary look-ups. For a given query image, it should be similar to its relative keys and dissimilar to others. MoCo split the encoder into an online network, updated by stochastic gradient descent, and a momentum network, updated on the exponential moving average of the online network weights. That allowed for smaller batch sizes (256 samples) but increased computational requirements.

BYOL [13] and SwAV [6] were the successful non-contrastive self-supervised techniques to beat contrastive techniques accuracy on standard benchmarks like ImageNet.

BYOL [13] mitigated the need for negative samples and, thus, larger batches sizes. The model used the same double-encoder design of MoCo, but added an extra MLP that attempts to predict the output of the momentum network from the output of the online network. BYOL’s authors suggested, with some empirical support, that the momentum network had a role in avoiding model collapse in the absence of negative samples.

SwAV [6] employs a clustering task as pretext, aiming at assigning views from the same image to the same cluster. It uses optimal transport [10] to assign the features extracted from the images to one of  $K$  cluster prototypes. The model does not degenerate to the trivial solution where all representations are assigned to a single cluster because the optimal transport algorithm encourages uniformly distributed features across clusters, avoiding trivial solutions by modeling a clustering assignment problem as a transportation polytope [6].

All methods presented so far use data augmentation to create views, but there are other possibilities. InfoMin [31] used labeled and unlabeled data to learn a view-generation network, by minimizing the mutual information between distinct views (luminance and chrominance channels from YDbDr color space), while ensuring to classify the object from each view. InfoMin uses the same self-supervised training as SimCLR, plugging the learned view generator in place of data augmentation. How to properly create optimal positive and negative views is still an open question [19, 31].

## 2.2 Self-supervised learning on medical tasks

Suitable pretext tasks are crucial for learning predictive representations. A few works were motivated by the question on whether domain-specific pretext tasks could improve the performance of self-supervised learning for medical images.

According to the survey by Jing et al. [19], mentioned earlier, the pretext tasks for images may be either *generative-based*, when they learn image features by generating or synthesize images, or *context-based*, when they use context-attributes such as the shape of objects, relative positions of parts of objects, or semantics among similar images.

Following the generative-based tasks, Chen *et al.* [7], and Hervella *et al.* [16] both investigate the context restoration [25] as self-supervised pretext task for, respectively, magnetic resonance and retinal images. Given an image sample, two randomly small image patches are selected and swapped or occluded. Repeating this operation multiple times creates a new image where the spatial information is disrupted. Then, they train a neural network to reconstruct the original image input given the modified version by employing  $\ell_1$  or  $\ell_2$  loss.

Context-based pretext tasks seem to be the most popular way of pre-training used in the literature. Wenjia *et al.* [2] leverage the information freely available in DICOM (standard storage for radiography images) file to pre-train for the cardiac segmentation task. The pretext task consists in predicting and segmenting the anatomical position (obtained from the headers of DICOM files) of the heart plane. Jamaludin *et al.* [18] and Zhout *et al.* [36] both show implicit or explicit contrastive-based pre-training in latent space using Siamese network [5] or a teacher-student framework. In all cases above, using the pre-training step in a self-supervised manner always presented advantages on the evaluated metrics. In some scenarios, using models trained only in-domain images showed better results than transfer learning from ImageNet [36].

## 2.3 Self-supervised learning on skin lesion analysis

Wang *et al.* [33] combined an  $\ell_2$ -reconstructing autoencoder and a transformation-invariant loss to encourage representations from two versions of the same skin lesion to be close in the latent space. They used the images nearest neighbors in latent space to build a graph, which they clustered into  $K$  groups based on a modularity clustering-quality metric. Pseudo-labels are generated according to the assigned cluster. They trained an additional network to predict the cluster assignment for each latent representation (node in the graph). The network is not entirely self-supervised, as the main encoder is transferred from a model fully-supervised on ImageNet. The evaluation of the pre-trained model uses the ISIC 2018 in a 7-class classification setup. The results showed that the self-supervised pre-trained only (without any fine-tuning) achieved 80.6% of accuracy score, a drop of 11.1pp in the same metric than fully-supervised baselines transferred from ImageNet fine-tuned on ISIC 2018. This suggests that only performing the pre-training can produce class-specific features without any label information.

Azizi *et al.* [1] used SimCLR to pre-train several skin-lesion diagnosis model, using a private dataset with over 450,000 clinical images from an array of different conditions. On such dataset, they obtain promising results, with self-supervised learning always improving both the accuracy and the AUC of evaluated models. As additional metadata information is available for another and smaller skin lesion dataset (over 15k samples), a new pre-training stage is performed by leveraging images from multiple viewpoints taken from the same patient. They use the patient ID metadata to sample two random images and create positive pairs, independently of skin condition and body parts. However, minimize the representations between intra-lesion images can even harm classification to spot hard clinical cases, especially treating of ugly ducklings [28].

## 3 Materials and methods

This section details the methodology, comprising the datasets and factors present in our experimental design. We also discuss how we conduct the experiments regarding all evaluated pipelines.

### 3.1 Datasets

Following the ISIC 2020 Challenge [27], our task is melanoma *vs.* benign lesions classification. We evaluate our experiments in five, high-quality, publicly available datasets (Table 1).

We performed all training and validation in splits of the isic19 dataset. We removed samples from isic20 that were present in the isic19 train/validation splits to avoid contaminating the former. We removed basal cell carcinomas and squamous cell carcinomas from all datasets, leaving melanoma as the only malignant class.

The diversity of test datasets allowed was aimed at mitigating bias in evaluation [3,4,11], providing both in-distribution (same dataset, same type of image, same classes) and out-of-distribution (cross-dataset, different types of image, different classes) scenarios.

Dataset	Size	Mel.	Lesion diagnoses	Other information
isic19 [9] train split†	14 805	3121	Melanoma vs. actinic keratosis, benign keratosis, dermatofibroma, melanocytic nevus, vascular lesion	Dermoscopic images.
isic19 [9] val. split†	1 931	224	Idem	Dermoscopic images, in-distribution.
isic19 [9] test split	3 863	396	Idem	Idem.
isic20 [27]	1 743	581	Melanoma vs. actinic keratosis, benign keratosis, lentigo, melanocytic nevus, unknown (benign)	Dermoscopic images, out-of-distribution, additional unknown diagnosis.
derm7pt–derm [20]	872	252	Melanoma vs. melanocytic nevus, seborrhoeic keratosis	Dermoscopic images, out-of-distribution.
derm7pt–clinic [20]	839	248	Melanoma vs. melanocytic nevus, seborrhoeic keratosis	Clinical images, out-of-distribution.
pad-ufes-20 [24]	1 261	52	Melanoma vs. actinic keratosis, Bowen’s disease, nevus, seborrheic keratosis	Clinical images, out-of-distribution, additional Bowen’s disease diagnosis.

Table 1: Description of the datasets used in this work. †All other splits/datasets used for test.

### 3.2 Model, pipelines, and self-supervised schemes

We follow the standard guidelines for self-supervised learning literature [29] and use the ResNet-50 (1 $\times$ ) [15] as the base encoder for all experiments.

We evaluate four alternative pipelines (Fig. 1), which vary in how the model is pre-trained and fine-tuned. All pipelines finish with a fine-tuning (FT) on the isic19 train split. The traditional supervised pipeline (SUP  $\rightarrow$  FT) is pre-trained using classical, supervised learning on ImageNet. All self-supervised pipelines (SSL  $\rightarrow$  \*) are pre-trained using self-supervision (without class annotations) on ImageNet. The SSL  $\rightarrow$  \*  $\rightarrow$  FT pipelines have an additional, intermediate pre-training step on the isic19 train split using supervised (UCL) or unsupervised (SCL) contrastive loss.

### 3.3 Experimental design

First, we wish to compare the baseline pipeline (SUP  $\rightarrow$  FT) with the basic self-supervision pipeline (SSL  $\rightarrow$  FT), to establish whether self-supervision is advantageous. In addition, we wish to select a self-supervision scheme among five candidates (BYOL, InfoMin, MoCo, SimCLR, and SwAV) to perform the remainder of the experiments. Selecting the most promising scheme at this stage is necessary to make the amount of experiments to run manageable, as the next round of experiments will be systematic and expensive.

In this first batch of experiments, we attempt a few combinations of hyperparameters for each self-supervision scheme. We purposefully optimize the baseline pipeline more thoroughly, in order to make it challenging. The exact search space appears in Sec. 3.4. We perform all search on the isic19 validation split, to avoid using privileged test information on this step [32]. To estimate the statistical significance of those experiments, we perform five replicates for every experiment, reflecting different random initializations for the training procedures (optimizer, scheduler, and augmentations).

The next round of experiments is a systematic evaluation of all pipelines (Sec 3.2 and Fig. 1) under three data regimens: full training data with 100% of the samples, and low training data with 10, and 1% of the samples. The latter intends to simulate the frequent scenario on medical images of insufficient training data.

On the double-pre-trained ones (SSL  $\rightarrow$  SCL/UCL  $\rightarrow$  FT) we vary batch sizes (80 or 512), balancing for the batches (yes or no), SimCLR temperature scale (0.1, 0.5 or 1), and training length (50 or 200 epochs). On the single-pre-trained (SSL  $\rightarrow$  FT) we varied the choice of the self-supervised model (SimCLR, MoCo, BYOL, SwAV, InfoMIN), and fine-tuning learning rate (0.01 or 0.001). On the baseline (SUP  $\rightarrow$  FT) pipeline, we varied batch size (32, 128, 512), balanced batches (yes or no), learning rate (0.1, 0.05, 0.005, 0.009, 0.0001), and learning rate scheduler (plateau, cosine).

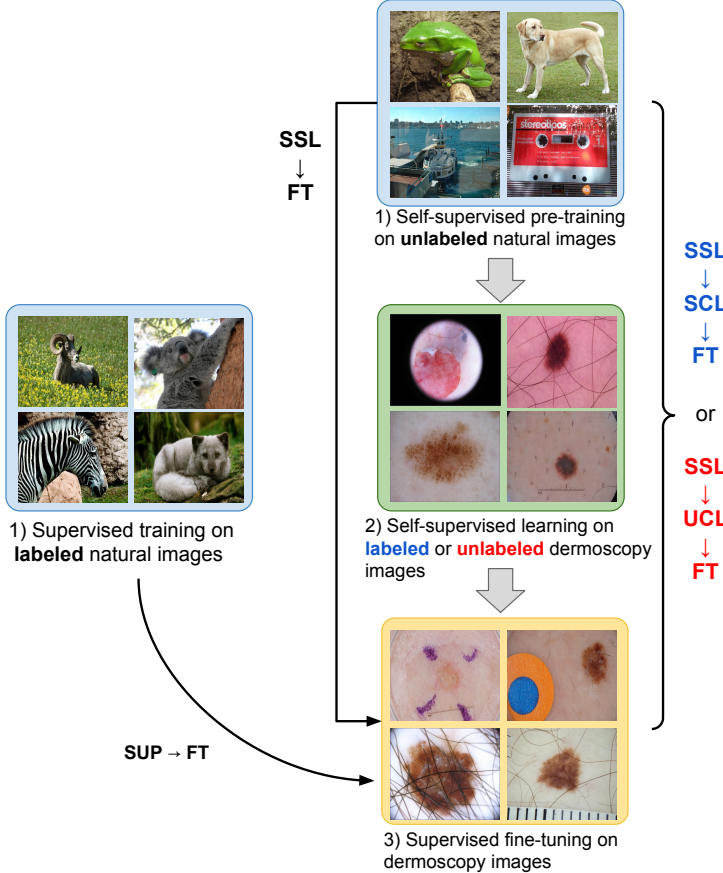


Figure 1: An overview of our evaluated pipelines. In SSL → FT scheme we contrast the result of five fine-tuned SSL ImageNet pre-trained models on isic19 dataset (see Section 3.7) with the supervised counterpart. The SSL → SCL → FT pipeline differs from SSL → UCL → FT according to the employed contrastive loss. They both go through a pre-training stage (see Section 3.6) — which can be supervised (SCL) or unsupervised (UCL) — using the isic19 dataset and then performing a supervised fine-tuning.

For each combination of pipeline and hyperparameters, we measure their performance on the isic19 validation split five times reflecting different random initializations for the training procedures, and, on the low-data experiments, different random training subsets. We pick the five non-unique best combinations of hyperparameters for each pipeline, and for each combination, we perform five replicates on the isic19 test split, resulting in 25 measurements for each pipeline.

### 3.4 SUP → FT baseline pipeline

In this pipeline, we start from ResNet-50 model pre-trained with a classical supervised loss on ImageNet and perform a fine-tuning, using a supervised loss on the isic19 training split.

We strive to make the baseline challenging, by performing, on the isic19 validation split, a thorough a grid search comprising batch size (32, 128, 512), balanced batches (yes or no), starting learning rate (0.1, 0.05, 0.005, 0.009, 0.0001), and learning rate scheduler (plateau, cosine). The optimizer is the SGD with a momentum of 0.9 and weight decay of 0.001. The plateau scheduler has a patience of 10 epochs and a reduction factor of 10. The fine-tuning lasts for 100 epochs with early stopping with a patience of 22 epochs, monitored on the validation loss. Both schedulers have a minimum learning rate of  $1e^{-5}$ .

### 3.5 SSL → FT pipeline

In this pipeline, we start from ResNet-50 model pre-trained with *self-supervised* losses on ImageNet and then perform a fine-tuning using a supervised loss on the isic19 training split.

We start from the best publicly available checkpoints for each of the self-supervised schemes we evaluate. For each model, we add a binary random-initialized linear layer to the output of the network, feeding to a cross-entropy loss function.

### 3.6 SSL → UCL/SCL → FT pipelines

Following SimCLR pre-training [8], we employ two fully-connected layers to embed the ResNet-50 onto 128-dimensional representations, which are fed to the contrastive loss. We resized the input images to  $224 \times 224$  and used SimCLR’s recommended heavy image augmentation pretexts — color jitter, horizontal and vertical flips, random resized crop, grayscale — but omitted the Gaussian blur because its effects on skin-lesion images lead to excessive loss of variation among images, harming the results. We used a learning rate of 0.001 with a cosine decay on an Adam optimizer. We initialized the model weights using the encoder checkpoint publicly available for ResNet-50 ( $1\times$ ) for SimCLR.

We evaluated two contrastive losses:

**Unsupervised Contrastive Loss (UCL):** we performed the pre-training using the self-supervised contrastive loss [8] on the isic19 training set. Only the image data is exploited, the annotations are not employed.

In unsupervised contrastive learning, the contrastive tasks involve model loss computation in the latent space by contrasting latent representations of positive and negative samples. Chen *et al.* [8] proposed a modified softmax-based named *NT-Xent* loss as follows:

$$\mathcal{L}_{UCL} = \sum_{i=1}^{2N} -\log \frac{\exp(\text{sim}(z_i, z_i^+)/\tau)}{\sum_{k=1}^{2N} \mathbb{1}_{i \neq k} \cdot \exp(\text{sim}(z_i, z_k^-)/\tau)}, \quad (1)$$

where  $z_j = f_\theta(x_j)$  is a normalized anchor latent vector representation of input image  $x_j$  parameterized by neural network  $f_\theta$  with respect of parameters  $\theta$ ,  $z_j^+$  and  $z_j^-$  are, respectively, positive and negative samples,  $\text{sim}(\cdot, \cdot)$  is any function that computes the similarity between two vectors,  $\mathbb{1}_B \in \{0, 1\}$  is an indicator function that returns 1 iff  $B$  evaluates as true,  $\tau > 0$  is a scalar temperature hyperparameter. Note that for each anchor  $j$ , there is a single positive pair and  $2N - 2$  negative samples.

**Supervised Contrastive Loss (SCL):** we performed pre-training using the supervised contrastive loss [22], which incorporates class label annotations, enhancing the semantic agreement between positive and negative pairs in the self-supervised samples.

Khosla et al. [22] extended the NT-Xent loss to its supervised version, allowing to use of multiple positive views or label information to create consistent positive and negative pairs. Its corresponding formulation is shown in Equation 2.

$$\mathcal{L}_{SCL} = -\frac{1}{N|P_i|} \sum_{i=1}^N \sum_{z_j \in P_i} -\log \frac{\exp(\text{sim}(z_i, z_j^+)/\tau)}{\sum_{z_k \in A_i} \exp(\text{sim}(z_i, z_k^-)/\tau)}, \quad (2)$$

where  $\tau$  is the temperature factor;  $P_i$  and  $A_i$  denote the positive pair set and the negative pairs set of the anchor  $z_i$ , respectively.  $|P_i|$  represents the cardinality of the set  $P_i$ , and  $N$  is the batch-size.

### 3.7 Final fine-tuning for all pipelines, Testing

We fine-tuning every model using an SGD optimizer with a momentum of 0.9 and weight decay of 0.001, and a plateau scheduler with a patience of 10 epochs and a reduction factor of 10. The fine-tuning lasts for 100 epochs with early stopping with a patience of 22 epochs, monitored on the validation loss. Notice that for the baseline pipeline, we performed additional optimizations (Sec. 3.4).

We resize input images to  $299 \times 299$ . Except for SimCLR, which uses raw inputs, we z-normalize the inputs per channel, with statistics from ImageNet. We augment training data with random horizontal and vertical flips, random resized crops containing from 75 to 100% of the original image, random rotations from  $-45$  to  $45^\circ$ , and random hue change from  $-20$  to  $20\%$ . We apply the same augmentations on train and validation. We also use test-time augmentations [32], averaging the predictions over 50 augmented versions of each test image [26].

### 3.8 Implementation details

We use PyTorch-Lightning<sup>1</sup> for the main development, PyContrast<sup>2</sup> for the self-supervised pre-trainings, and Comet.ML<sup>3</sup> for experiment management.

All experiments ran in a single RTX 5000 GPU, except for the SSL → UCL/SCL → FT pipelines on a 512-batch size, which required two Quadro RTX 8000 GPUs.

The ResNet-50 supervised pre-trained weights on ImageNet used on the baseline came from torchvision. For the z-normalization, we use the ImageNet RGB channel means (0.485, 0.456, 0.406), and standard deviations (0.229, 0.224, 0.225), in a range of [0, 1], also from torchvision.

The SimCLR pre-trained weights on ImageNet for ResNet-50 is obtained from the original repository<sup>4</sup>.

The original self-supervised models were pre-trained by their authors as follows. BYOL: batch size=4096, training length=1000 epochs (temperature parameter unused at pre-trained); InfoMin: batch size=256, temperature=0.07, training length=800 epochs; MoCo: batch size=256, temperature=0.07, training length=800 epochs; SimCLR: batch size=4096, temperature=0.1, training length=800 epochs; SwAV: batch size=4096, temperature=0.1, training length=800 epochs. All models are pre-trained on ImageNet.

The source code used in this work, in addition to detailed descriptions about the data is available on our source-code repository.<sup>5</sup>

## 4 Results

As explained in Sec. 3.3, we organized our extensive experimental design into two batches, corresponding to the next two subsections. In a third subsection, we analyze the second batch of experiments in the specific scenario of low training data.

Method	AUC %		Hyperparameters			
	Mean	Std	LR	batch	label	
Sup. baseline	948 ± 6		LR=0.009	batch=128	balanced	plateau
<b>SimCLR [8]</b>	<b>956 ± 3</b>		LR=0.01	batch=32	unbalanced	plateau
SwAV [6]	953 ± 6		LR=0.01	batch=32	unbalanced	plateau
BYOL [13]	946 ± 5		LR=0.01	batch=32	unbalanced	plateau
InfoMin [31]	944 ± 5		LR=0.001	batch=32	unbalanced	plateau
MoCo [14]	939 ± 7		LR=0.001	batch=32	unbalanced	plateau

Table 2: Results for the first batch of experiments, comparing the supervised SUP → FT baseline to the basic SSL → FT pipeline with five SSL schemes. The metric is the AUC on the isic19 validation split. Despite the baseline using label information on pre-training, and being more thoroughly optimized, self-supervision pre-training is still very competitive with it.

### 4.1 Self-supervision schemes vs. baseline comparison

In this first batch of experiments, we compared the baseline pipeline (SUP → FT) to the basic self-supervision pipeline (SSL → FT) with five self-supervision schemes (BYOL, InfoMin, MoCo, SimCLR, and SwAV). We optimized the baseline pipeline as explained in Sec. 3.4, and the self-supervised baselines as explained in Sec. 3.5. Finally, We fine-tuned both models for the final task as explained in Sec. 3.7.

The results (Table 2) show that, despite having no access to the labels during the pre-training, and being less thoroughly optimized during the final fine-tuning, the models with self-supervised pre-training are very competitive. Indeed, two of the pipelines (SimCLR and SwAV) had averages above the ones in the baseline.

This first batch of experiments intended to validate the applicability of self-supervised learning, and to select one self-supervised scheme for the expensive round of systematic evaluations in the next batch. Thus, it comes with the

<sup>1</sup><https://github.com/PyTorchLightning/pytorch-lightning>

<sup>2</sup><https://github.com/HobbitLong/PyContrast>

<sup>3</sup><https://www.comet.ml>

<sup>4</sup><https://github.com/google-research/simclr>

<sup>5</sup><https://github.com/VirtualSpaceman/ssl-skin-lesions>

important caveat that optimizations and evaluations were both conducted in the isic19 validation set. The second batch of experiments will evaluate the ability of the pipelines to generalize performance in the rigorous setting of a held-out test set.

## 4.2 Systematic evaluation of pipelines

In the second batch of experiments, we performed a systematic evaluation of the baseline pipeline, pre-trained with supervision ( $SUP \rightarrow FT$ ) against the three pipelines pre-trained with self-supervision ( $SSL \rightarrow FT$ ,  $SSL \rightarrow UCL \rightarrow FT$ , and  $SSL \rightarrow SCL \rightarrow FT$ ). In this batch, we only evaluated SimCLR as the self-supervision scheme, for several reasons: it showed the best performance in the preliminary experiments (Sec. 4.1), it allows introducing annotation information easily with a supervised contrastive loss, it had one hyperparameter less than SwAV to optimize (number of clusters), the ablation studies in the original papers helped to decide on a range of reasonable values for the temperature value.

We optimized the baseline pipeline as explained in Sec. 3.4, and the self-supervised baselines as explained in Sec. 3.5 and Sec. 3.6. We fine-tuned all models for the final task as explained in Sec. 3.7.

As explained in Sec. 3.3, this batch of experiments simulates a realistic machine-learning protocol, in which first we optimize the hyperparameters for each pipeline on the isic19 validation split, then evaluate the performance on a held-out test set. The test set may be the in-distribution isic19 test split, or the out-of-distribution isic20, derm7pt-derm, derm7pt-clinic, and pad-ufes20. Those cross-dataset evaluations are critical to evaluate how well the pipelines generalize to different classes, image acquisition techniques, or even to subtle dataset variations across institutions.

The results appear in the topmost plot of Fig. 2, where each boxplot shows the distribution of 25 individual measurements (small black dots), corresponding to the best five non-unique hyperparameterizations, with five replicates for each of them. The boxplots show, as usual, the three quartiles (box), and the range of the data (whiskers) up to  $1.5 \times$  the interquartile range (samples outside that range are plotted individually as “outliers”). The large red dots show the means for each experiment. The metric is the AUC on the test datasets labeled on the right vertical axis. To make the horizontal axis comparable across its domain, we linearize the AUC using the logit (i.e., the logarithm of the odds) is base 2, shown on the bottom axis. The original AUC values appear on the top axis.

The plots reveal two advantages for the self-supervised pipelines: first performances (means and medians) tend to be higher; second, the variability (width of the boxes) tended to be smaller. That shows the ability of the self-supervised pre-training not only in improving the results, but also in making them more stable.

No consistent advantage, in terms of trend improvement (mean, median) is evident among the different self-supervised pipelines, but in terms of variability reduction, the double-pre-trained pipelines ( $SSL \rightarrow SCL/UCL \rightarrow FT$ ) pipelines appear to have a slight advantage.

## 4.3 Low training data scenario

These results follow the same protocol as those in the previous section, but with drastically reduced train datasets. The results appear in the middle and bottom-most plots in Fig. 2, for 10% (1480 samples) and 1% (148 samples), respectively, of the original train dataset. Other than for this restriction, the interpretation of the plots is the same as in the previous section.

These results are much noisier than the full-data experiments, in part intrinsically due to the smaller training sets. In part, the replicates incorporate the variability due to the choice of a random subset of training data.

Again, the self-supervised pipelines appear advantageous, both in terms of trend improvement (mean, median) and in terms of variability reduction, but here the advantage of the double-pre-trained pipelines ( $SSL \rightarrow SCL/UCL \rightarrow FT$ ) seems more decisive, especially for the lowest data regimen, where it brings a clear improvement both in trend and variability. As we will discuss in the conclusions, this variability reduction is critical for the soundness of the deployment of low-data models.

## 5 Conclusions

Our experiments show that self-supervised pre-training makes models easier to deploy than classical supervised pre-training, since even with a less thorough hyperoptimization the former outperformed the latter, in general trends, and, especially in variability.

It is hard to quantify this impression, but the models pre-trained with self-supervised also “felt” easier, faster, more “ready-to-use” than the baseline models during training.

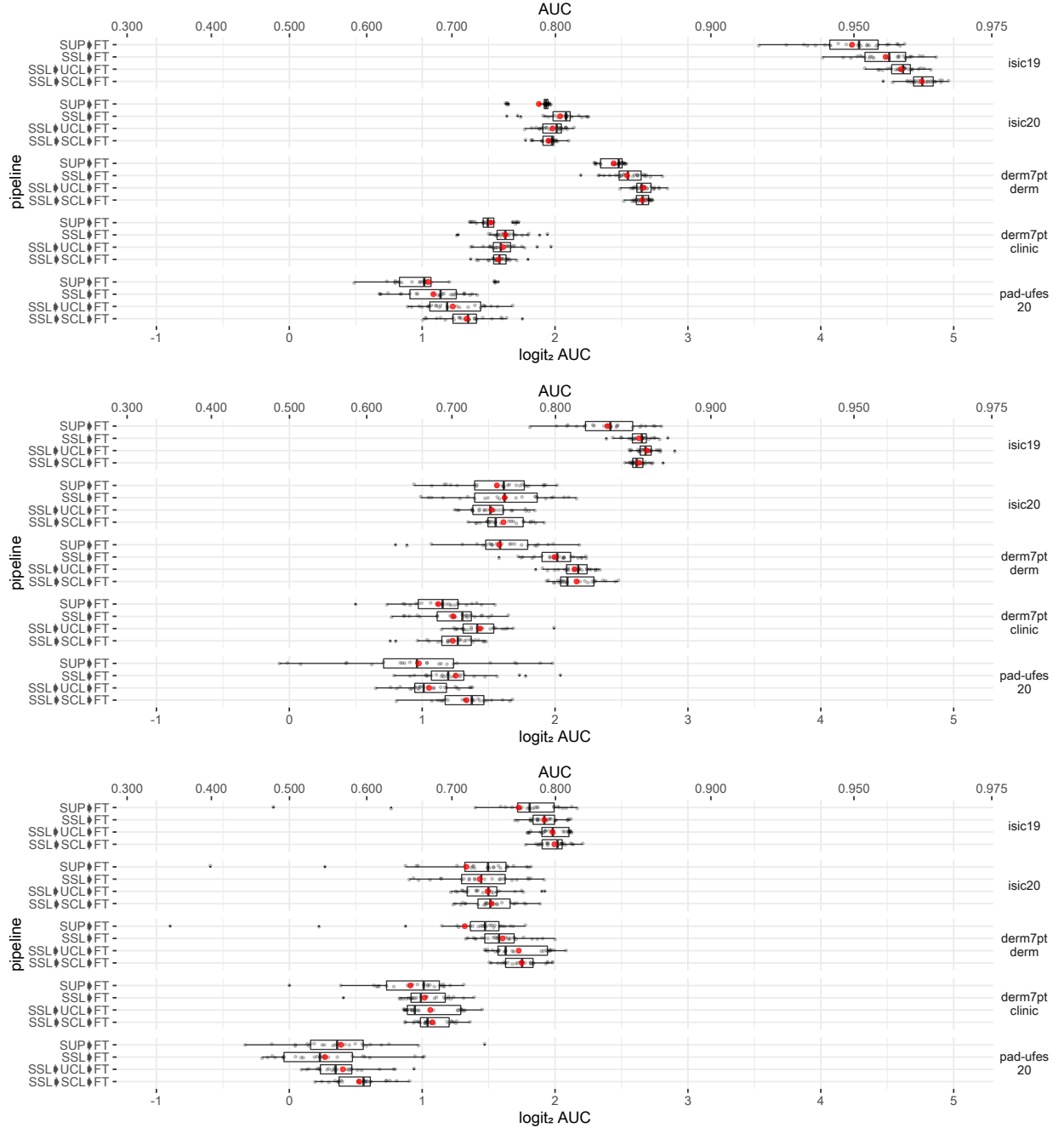


Figure 2: Results for the second batch of experiments, with a systematic comparison of the pipelines labeled on the left vertical axis at the datasets labeled on the right vertical axis. The top, middle, and bottom plots show results for 100, 10 and, 1% of the training data, respectively. Individual measurements represented by each boxplot appear as small black dots, whose means appear as larger red dots. In general, self-supervised pre-trained improves trends (medians, means) and reduces variability, both in the full-data and the low-data scenarios.

The advantage of the self-supervised pipelines was particularly prominent on the low-data scenarios, where their ability to stabilize the results, reducing variability was even more noticeable. In those scenarios, especially the very-low data one, the double-pre-trained models appeared advantageous.

Very low-data scenarios are not, unfortunately, rare on medical applications. Models trained on such regimens will experience large variances in performance in contrast to models trained with adequate samples, but, model designers will often be unaware of such variance (since they cannot run a simulation such as ours, comparing their model to others trained in different datasets of the same size). Our results suggest that self-supervised pre-training may reduce those variabilities, leading to saner models. Of course, models trained on small samples may suffer from severe biases, and extensive exploration is necessary to evaluate whether self-supervised might reinforce those biases [3].

Self-supervised learning is a thriving research area, and the possibility of creating domain-specific or at least domain-aware pretext tasks for skin-lesion analysis is an exciting avenue of continuation for this work. Even while using commodity pretext tasks, domain-aware sampling methods, for selecting the positive and negative pairs in contrastive learning, are also an instigating possibility of incorporating domain knowledge into self-supervision learning.

## Acknowledgements

L. Chaves is partially funded by QuintoAndar, and CAPES. A. Bissoto is partially funded by FAPESP 2019/19619-7. E. Valle is funded by CNPq 315168/2020-0. S. Avila is partially funded by CNPq PQ-2 315231/2020-3, and FAPESP 2013/08293-7. A. Bissoto and S. Avila are also partially funded by Google LARA 2020. RECOD Lab. is supported by projects from FAPESP, CNPq, and CAPES. We acknowledge the donation of GPUs by NVIDIA.

## References

- [1] AZIZI, S., MUSTAFA, B., RYAN, F., BEAVER, Z., FREYBERG, J., DEATON, J., LOH, A., KARTHIKE-SALINGAM, A., KORNBLITH, S., CHEN, T., ET AL. Big self-supervised models advance medical image classification. *arXiv preprint arXiv:2101.05224* (2021). 1, 3
- [2] BAI, W., CHEN, C., TARRONI, G., DUAN, J., GUITTON, F., PETERSEN, S. E., GUO, Y., MATTHEWS, P. M., AND RUECKERT, D. Self-supervised learning for cardiac mr image segmentation by anatomical position prediction. In *Medical Image Computing and Computer Assisted Intervention* (2019), pp. 541–549. 3
- [3] BISSOTO, A., FORNACIALI, M., VALLE, E., AND AVILA, S. (de)constructing bias on skin lesion datasets. In *Conference on Computer Vision and Pattern Recognition Workshops* (2019). 4, 10
- [4] BISSOTO, A., VALLE, E., AND AVILA, S. Debiasing skin lesion datasets and models? not so fast. In *Conference on Computer Vision and Pattern Recognition Workshops* (2020), pp. 740–741. 4
- [5] BROMLEY, J., GUYON, I., LECUN, Y., SÄCKINGER, E., AND SHAH, R. Signature verification using a "siamese" time delay neural network. In *Advances in Neural Information Processing Systems* (1994). 3
- [6] CARON, M., MISRA, I., MAIRAL, J., GOYAL, P., BOJANOWSKI, P., AND JOULIN, A. Unsupervised learning of visual features by contrasting cluster assignments. In *Advances in Neural Information Processing Systems* (2020), pp. 9912–9924. 1, 2, 7
- [7] CHEN, L., BENTLEY, P., MORI, K., MISAWA, K., FUJIWARA, M., AND RUECKERT, D. Self-supervised learning for medical image analysis using image context restoration. *Medical Image Analysis* 58 (2019), 101539. 3
- [8] CHEN, T., KORNBLITH, S., NOROZI, M., AND HINTON, G. A simple framework for contrastive learning of visual representations. In *International Conference on Machine Learning* (2020). 1, 2, 6, 7
- [9] CODELLA, N., GUTMAN, D., CELEBI, M. E., HELBA, B., MARCHETTI, M. A., ET AL. Skin lesion analysis toward melanoma detection: A challenge at the 2017 international symposium on biomedical imaging (isbi), hosted by the international skin imaging collaboration (isic). In *International Symposium on Biomedical Imaging* (2018), pp. 168–172. 4
- [10] CUTURI, M. Sinkhorn distances: Lightspeed computation of optimal transport. In *Advances in Neural Information Processing Systems* (2013), pp. 2292–2300. 2
- [11] GEIRHOS, R., JACOBSEN, J.-H., MICHAELIS, C., ZEMEL, R., BRENDEL, W., BETHGE, M., AND WICHMANN, F. A. Shortcut learning in deep neural networks. *Nature Machine Intelligence* 2, 11 (2020), 665–673. 4

- [12] GIDARIS, S., SINGH, P., AND KOMODAKIS, N. Unsupervised representation learning by predicting image rotations. *International Conference on Learning Representations* (2018). [2](#)
- [13] GRILL, J.-B., STRUB, F., ALTCHÉ, F., TALLEC, C., RICHEMOND, P., BUCHATSKAYA, E., DOERSCH, C., AVILA PIRES, B., GUO, Z., GHESHLAGHI AZAR, M., PIOT, B., KAVUKCUOGLU, K., MUNOS, R., AND VALKO, M. Bootstrap your own latent - a new approach to self-supervised learning. In *Advances in Neural Information Processing Systems* (2020), pp. 21271–21284. [1, 2, 7](#)
- [14] HE, K., FAN, H., WU, Y., XIE, S., AND GIRSHICK, R. Momentum contrast for unsupervised visual representation learning. In *Conference on Computer Vision and Pattern Recognition* (2020). [1, 2, 7](#)
- [15] HE, K., ZHANG, X., REN, S., AND SUN, J. Deep residual learning for image recognition. In *Conference on Computer Vision and Pattern Recognition* (2016), pp. 770–778. [4](#)
- [16] HERVELLA, Á. S., ROUCO, J., NOVO, J., AND ORTEGA, M. Retinal image understanding emerges from self-supervised multimodal reconstruction. In *Medical Image Computing and Computer Assisted Intervention* (2018), pp. 321–328. [3](#)
- [17] HU, D., QIAN, R., JIANG, M., TAN, X., WEN, S., DING, E., LIN, W., AND DOU, D. Discriminative sounding objects localization via self-supervised audiovisual matching. In *Advances in Neural Information Processing Systems* (2020), vol. 33, pp. 10077–10087. [1](#)
- [18] JAMALUDIN, A., KADIR, T., AND ZISSERMAN, A. Self-supervised learning for spinal mrис. In *MICCAI Workshop on Deep Learning in Medical Image Analysis*. 2017, pp. 294–302. [3](#)
- [19] JING, L., AND TIAN, Y. Self-supervised visual feature learning with deep neural networks: A survey. *IEEE Transactions on Pattern Analysis and Machine Intelligence* (2020). [2, 3](#)
- [20] KAWAHARA, J., DANESHVAR, S., ARGENZIANO, G., AND HAMARNEH, G. Seven-point checklist and skin lesion classification using multitask multimodal neural nets. *IEEE Journal of Biomedical and Health Informatics* 23, 2 (2019), 538–546. [4](#)
- [21] KAWAKAMI, K., WANG, L., DYER, C., BLUNSOM, P., AND OORD, A. v. d. Learning robust and multilingual speech representations. *arXiv preprint arXiv:2001.11128* (2020). [1](#)
- [22] KHOSLA, P., TETERWAK, P., WANG, C., SARNA, A., TIAN, Y., ISOLA, P., MASCHINOT, A., LIU, C., AND KRISHNAN, D. Supervised contrastive learning. In *Advances in Neural Information Processing Systems* (2020), pp. 18661–18673. [6](#)
- [23] MENEGOLA, A., FORNACIALI, M., PIRES, R., BITTENCOURT, F. V., AVILA, S., AND VALLE, E. Knowledge transfer for melanoma screening with deep learning. In *International Symposium on Biomedical Imaging* (2017), pp. 297–300. [1](#)
- [24] PACHECO, A. G., LIMA, G. R., SALOMÃO, A. S., KROHLING, B., BIRAL, I. P., DE ANGELO, G. G., ALVES JR, F. C., ESGARIO, J. G., SIMORA, A. C., CASTRO, P. B., ET AL. Pad-ufes-20: A skin lesion dataset composed of patient data and clinical images collected from smartphones. *Data in brief* 32 (2020), 106221. [4](#)
- [25] PATHAK, D., KRAHENBUHL, P., DONAHUE, J., DARRELL, T., AND EFROS, A. A. Context encoders: Feature learning by inpainting. In *Conference on Computer Vision and Pattern Recognition* (2016), pp. 2536–2544. [2, 3](#)
- [26] PEREZ, F., VASCONCELOS, C., AVILA, S., AND VALLE, E. Data augmentation for skin lesion analysis. In *OR 2.0 Context-Aware Operating Theaters, Computer Assisted Robotic Endoscopy, Clinical Image-Based Procedures, and Skin Image Analysis*. 2018. [6](#)
- [27] ROTEMBERG, V., KURTANSKY, N., BETZ-STABLEIN, B., CAFFERY, L., CHOUSAOKOS, E., CODELLA, N., COMBALIA, M., DUSZA, S., GUITERA, P., GUTMAN, D., ET AL. A patient-centric dataset of images and metadata for identifying melanomas using clinical context. *Scientific data* 8, 1 (2021), 1–8. [3, 4](#)
- [28] SOENKSEN, L. R., KASSIS, T., CONOVER, S. T., MARTI-FUSTER, B., BIRKENFELD, J. S., TUCKER-SCHWARTZ, J., NASEEM, A., ET AL. Using deep learning for dermatologist-level detection of suspicious pigmented skin lesions from wide-field images. *Science Translational Medicine* 13, 581 (2021). [3](#)
- [29] SRIKAR APPALARAJU, YI ZHU, Y. X., AND FEHERVARI, I. Towards good practices in self-supervised representation learning. In *Advances in Neural Information Processing Systems Workshops* (2020). [4](#)
- [30] TACK, J., MO, S., JEONG, J., AND SHIN, J. Csi: Novelty detection via contrastive learning on distributionally shifted instances. In *Advances in Neural Information Processing Systems* (2020), pp. 11839–11852. [2](#)
- [31] TIAN, Y., SUN, C., POOLE, B., KRISHNAN, D., SCHMID, C., AND ISOLA, P. What makes for good views for contrastive learning? In *Advances in Neural Information Processing Systems* (2020). [1, 2, 7](#)

- [32] VALLE, E., FORNACIALI, M., MENEGOLA, A., TAVARES, J., BITTENCOURT, F. V., LI, L. T., AND AVILA, S. Data, depth, and design: Learning reliable models for skin lesion analysis. *Neurocomputing* 383 (2020), 303–313. [1](#), [4](#), [6](#)
- [33] WANG, D., PANG, N., WANG, Y., AND ZHAO, H. Unlabeled skin lesion classification by self-supervised topology clustering network. *Biomedical Signal Processing and Control* 66 (2021), 102428. [1](#), [3](#)
- [34] WU, Z., XIONG, Y., YU, S. X., AND LIN, D. Unsupervised feature learning via non-parametric instance discrimination. In *Conference on Computer Vision and Pattern Recognition* (2018). [2](#)
- [35] ZHANG, R., ISOLA, P., AND EFROS, A. A. Colorful image colorization. In *European Conference on Computer Vision* (2016), pp. 649–666. [2](#)
- [36] ZHOU, H.-Y., YU, S., BIAN, C., HU, Y., MA, K., AND ZHENG, Y. Comparing to learn: Surpassing imagenet pretraining on radiographs by comparing image representations. In *Medical Image Computing and Computer Assisted Intervention* (2020), pp. 398–407. [1](#), [3](#)